Biosensors Hot Paper

Deutsche Ausgabe: DOI: 10.1002/ange.201505712
Internationale Ausgabe: DOI: 10.1002/anie.201505712

Electronic Olfactory Sensor Based on *A. mellifera* Odorant-Binding Protein 14 on a Reduced Graphene Oxide Field-Effect Transistor

*Melanie Larisika, Caroline Kotlowski, Christoph Steininger, Rosa Mastrogiacomo, Paolo Pelosi, Stefan Schütz, Serban F. Peteu, Christoph Kleber, Ciril Reiner-Rozman, Christoph Nowak, and Wolfgang Knoll**

Abstract: *An olfactory biosensor based on a reduced graphene oxide (rGO) field-effect transistor (FET), functionalized by the odorant-binding protein 14 (OBP14) from the honey bee (Apis mellifera) has been designed for the in situ and real-time monitoring of a broad spectrum of odorants in aqueous solutions known to be attractants for bees. The electrical measurements of the binding of all tested odorants are shown to follow the Langmuir model for ligand–receptor interactions. The results demonstrate that OBP14 is able to bind odorants even after immobilization on rGO and can discriminate between ligands binding within a range of dissociation constants from $K_d = 4\,\mu$M to $K_d = 3.3$ mM. The strongest ligands, such as homovanillic acid, eugenol, and methyl vanillate all contain a hydroxy group which is apparently important for the strong interaction with the protein.*

Odorant-binding proteins (OBPs) are small acidic proteins (ca. 13–16 kDa) highly concentrated in the lymph of the chemosensillae of insects or in the nasal mucus of vertebrates.[1] They act as carriers for volatile organic compounds, VOCs, (air-borne odorants) shuttling them from the air–water interface to the membrane-integral odorant receptor. Although their full function has not been completely clarified yet, OBPs certainly play a major role in detecting and recognizing olfactory stimuli.[2]

A large number of OBPs has been expressed in bacterial systems and their ligand-binding properties have been investigated in solution by a fluorescent ligand displacement assay.[3] Generally, dissociation constants, K_d, are in the upper nanomolar or lower micromolar range for strong odorants.[1c,d] An important characteristic of OBPs for technical applications is their stability to extreme temperatures, solvents, and proteolysis, making such proteins ideal elements for biosensors to be used in medical application, for example, in breath analysis for cancer diagnostics, for food quality control, for crop-disease detection, or in general environmental monitoring.[4a–f]

Various biosensor devices mimicking the olfactory system (artificial noses) have been developed but only few studies have used OBPs as functional elements for the design of a "bio-electronic nose".[5] Herein we present the fabrication and functional characterization of a label-free biosensor for odorant detection based on a reduced graphene oxide field-effect transistor functionalized with the odorant-binding protein 14 (OBP14) from the honey bee *Apis mellifera*.

Reduced graphene oxide field-effect transistor (rGO-FET) devices were fabricated according to established methods, schematically given in Figure 1 A.[6] A scanning electron microscopic image of rGO flakes assembled onto the gate substrate before any further surface functionalization is shown in Figure 1 B. IR spectra of the linker monolayer, 1-pyrenebutanoic acid succinimidyl ester (PBSE), that is typically used for protein immobilization on graphene substrates,[7] with partial covalent immobilization of OBP taken at different times during the assembly from solution to the gate are given in Figure 1 C, while Figure 1 D summarizes the quantitative analysis of the functionalization process by monitoring the time-dependent increase of the amide I and II bands of the protein and the corresponding decrease of the band at 1738 cm^{-1}, assigned to the cleavage of the active ester group of the linker molecules. The entire fabrication process of the olfactory biosensor device, including the successful reduction of GO to rGO, the linker binding, and more details of the protein attachment are described in the Supporting Information. The cloning, expression, and purification of OBPs, the preparation of odorant solutions and the performance of the electrical measurements are also described in the Supporting Information.

The mode of operation of the device as a field-effect transistor is demonstrated in Figure S5. Recording the I_{SD} versus V_G scans under different bulk solution conditions, in

[*] Dr. M. Larisika,[+] C. Kotlowski,[+] C. Steininger, C. Reiner-Rozman, Dr. C. Nowak, Prof. W. Knoll
BioSensor Technologies
Austrian Institute of Technology
Vienna (Austria)
E-mail: wolfgang.knoll@ait.ac.at

Dr. M. Larisika,[+] Dr. C. Nowak, Prof. W. Knoll
Centre for Biomimetic Sensor Science
Nanyang Technological University
Singapore 637371 (Singapore)

C. Kotlowski,[+] Prof. C. Kleber, C. Reiner-Rozman, Dr. C. Nowak, Prof. W. Knoll
Center for Electrochemical Surface Technology
Wiener Neustadt (Austria)

R. Mastrogiacomo, Prof. P. Pelosi
Department of Biology of Agriculture, Food and Environment
University of Pisa (Italy)

Prof. S. Schütz
Buesgen-Institute, Dept. of Forest Zoology and Forest Conservation
Goettingen (Germany)

S. F. Peteu
Michigan State University
Chemical Engineering & Materials Science (USA)

[+] These authors contributed equally to this work.

Supporting information for this article is available on the WWW under http://dx.doi.org/10.1002/anie.201505712.

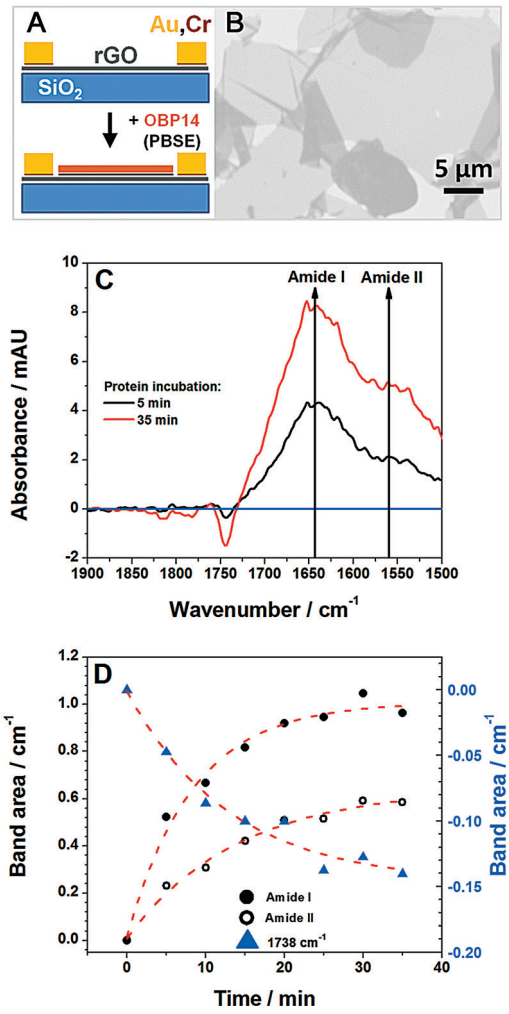

Figure 1. A) Schematic illustration of the individual fabrication steps of the graphene biosensor device. B) Scanning electron microscopic image of the rGO-FET before the functionalization with 1-pyrene-butanoic acid succinimidyl ester (PBSE) linker. C) Infrared spectra of the PBSE linker attached to gate area of the rGO surface, and OBP14 immobilized for 5 and 35 min, respectively, as indicated (spectra measured in ATR configuration and water corrected). D) Time-dependent increase of the amide I and II bands, upon binding of OBP14 to the linker molecules at the gate surface, and the corresponding decrease of the band at 1738 cm^{-1} upon cleavage of the active ester of the linker molecules during the protein immobilization (cf. also Figure S6). The dashed red curves are guides to the eye.

particular, in aqueous solutions with different ligand concentrations results in a slightly modified slope of the cathodic branch. We attribute this change to a slight modification of the dipolar layer upon binding of the ligands to the free binding sites in the OBP which act as receptors. The OBP protein monolayer is immobilized on the graphene gate and ligand binding causes a the slight reorientation of its the alpha-helical parts. At the selected gate voltage of $V_G = -0.6$ V the concentration dependency of the slopes in the I_{SD} versus V_G curves could be used to measure the binding of odorants to OBP14 in real-time, resulting in the quantitative determination of the kinetic rate constants for the association process, k_{on}, and for the dissociation process, k_{off}, as well as for the affinity constant K_A and the dissociation constant K_d. As an example, Figure 2 A shows a global analysis measurement, that is, the time dependence of the change of the source-drain current, ΔI_{SD}, of the FET as a function of time upon binding of methyl vanillate, a strong binder, from solution to the OBP14-functionalized gate surface at increasing and decreasing odorant bulk concentrations. The error of the kinetic rate

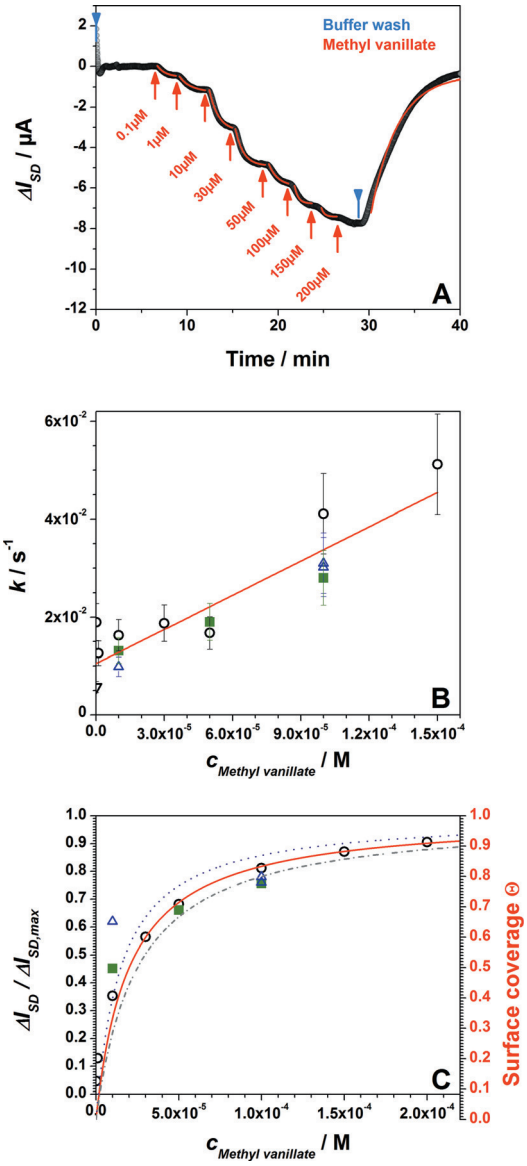

Figure 2. A) Real-time biosensor measurement of the binding of methyl vanillate to OBP14: the current increases with the bulk concentration of methyl vanillate increasing (from 100 nM to 200 µM) and then saturates. Blue arrows indicate runs with pure buffer, red arrows indicate experiments with methyl vanillate solutions. Red curves are the fitting of the raw data by kinetic simulations of the association and dissociation processes based on the Langmuir model. (For the estimation of the error limits, see the Supporting Information). B) Analysis of the reaction rate constants, k, obtained from the fitted data in (A) as a function of methyl vanillate concentration; different symbols from three different devices; error bars are ±20%. C) Langmuir adsorption isotherm, obtained for three different samples; the red fit curve gives $K_d = 20$ µM (plotted are also error limits for K_d of 20%).

constants, k, obtained was estimated to be around 20% (cf. also Figure S8 in the Supporting Information).

Upon plotting the resulting reaction rate constants k, as they were derived from the fits to the kinetic traces as a function of the bulk ligand concentration, $c_0 = c_{\text{Methyl vanillate}}$, (Figure 2B), gives a straight line, the slope of which, according to $k = k_{on} c_0 + k_{off}$, with k_{on} being the association and k_{off} the dissociation rate constant, respectively, yields $k_{on} = 235\,\text{M}^{-1}\text{s}^{-1}$, and the intersection with the y-axis gives $k_{off} = 0.01\,\text{s}^{-1}$. According to the Langmuir model the ratio k_{on}/k_{off} gives the affinity constant $K_A = 2.3 \times 10^4\,\text{M}^{-1}$, which can be compared to the value derived from the equilibrium titration experiment given in Figure 2C: according to $\theta = K_A c_0/(1 + K_A c_0)$ the fit to the data (full red curve plus the error limits of $\pm 20\%$) gives the affinity constant $K_A = 5 \times 10^4\,\text{M}^{-1}$ which compares quite well with the value obtained from the kinetic experiments thus confirming the Langmuir model for this binding process.

To exclude false signals arising from, in particular, non-specific binding, several control experiments were performed. Firstly, a sensor was prepared which was covered only with linker molecules, without the coupling of the odorant-binding protein. Even high concentrations of the strong binder homovanillic acid (cf. Figure S7A) or other ligands (Figure S7B) did not result in a significant signal. Coating the gate with OBP14 but exposing it to a totally uncorrelated small molecule, biotin, gave no signal (Figure S7C). And finally, immobilizing a protein (OBP9A from the red flour beetle, *Tribolium castaneum*) that is structurally similar but is not a receptor for these ligand odorants also gave a very weak signal (Figure S7D).

Further evidence for the specificity of the ligand receptor binding originates from a direct comparison of the binding of eugenol and methyl eugenol to the same chip, functionalized with OBP14. Figure 3A shows a real-time current trace recorded during the addition of methyl eugenol at 50 μM, then rinsing with pure buffer, and then a 5 μM solution of eugenol being rinsed through the flow cell. Despite the minor chemical variation between the two ligands a large difference in the affinity of their binding reaction to OBP14 confirms the specificity of the sensor. Figure 3B summarizes the Langmuir isotherms for both ligands, demonstrating the significantly

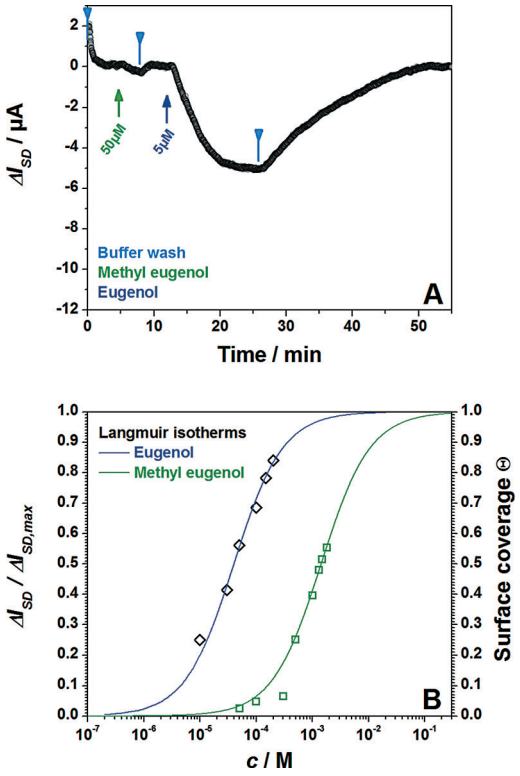

Figure 3. A) Real-time sensor response to the injection of a 50 μM solution of methyl eugenol, subsequent buffer wash, and the injection of 5 μM eugenol solution. B) Langmuir isotherms of eugenol and methyl eugenol.

different dissociation constants: $K_d = 40$ μM for eugenol and $K_d = 1400$ μM for methyl eugenol.

Table 1 summarizes the quantitative data measured for a series of ligands and gives the kinetic rate constants, k_{on} and k_{off}, obtained as well as the dissociation constant K_d. It could be confirmed also for this label-free sensing format that the odorant binding affinity to OBP14 gradually decreases from homovanillic acid to citral and to geraniol.[8] Molecules which are structurally related to eugenol also showed strong affinities to OBP14.

Table 1: Dissociation constants, K_d, association rate constants, k_{on}, and dissociation rate constants, k_{off}, for a variety of odorants binding to OBP14 as obtained by the global analysis.

Odorant	Homovanillic acid	Methyl vanillate	Eugenol	Citral	Methyl eugenol	Geraniol
structural formula	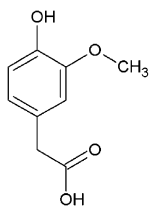	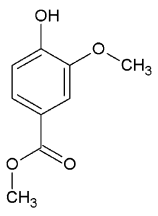	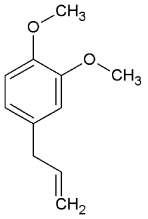	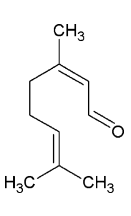	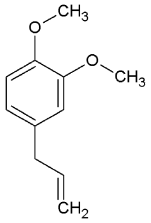	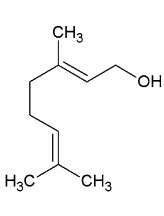
K_d [$\times 10^{-6}$ M]	4	20	40	800	1400	3300
k_{on} [$\text{M}^{-1}\text{s}^{-1}$]	1130	235	170	9	6	3
k_{off} [s^{-1}]	0.008	0.01	0.006	0.003	0.006	0.008

Interestingly, also other odorant-binding proteins bind their odorants with affinities in the same order of magnitude.[9] It is remarkable to note that for all the ligands investigated the dissociation rate constants k_{off}, differ by less than a factor of 2.5. The strongly differing affinity constants, varying by nearly three orders of magnitude, can be almost exclusively attributed to the differences in the association rate constants k_{on}, (cf. Table 1).

The Spinelli group used X-ray diffraction analysis to determine the structure of the eugenol–OBP14 complex. They found that the hydroxy group of eugenol interacts with the cavity wall of the OBP14 binding pocket by forming two hydrogen bonds.[10]

It has been speculated that the hydroxy group, together with the substituted aromatic backbone, plays a key role for the strong binding which is in agreement with the high affinities also of homovanillic acid and methyl vanillate (cf. Table 1).[10] This hypothesis is further supported by the lower affinity measured for methyl eugenol, in which the hydroxy group is replaced by a methoxy group.

Acknowledgements

This research is supported by the European Science Foundation (ESF), Grant Number: 10-EuroBioSAS-FP-005, by the FFG within the comet program, and from the governments of Lower and Upper Austria. We thank Prof. Lendl (Technical University of Vienna) and his group (Christoph Gasser, Georg Ramer, Karin Wieland) for technical support regarding Raman and FTIR measurements.

Keywords: biosensors · immobilization · odorant-binding protein · olfaction · reduced graphene oxide

How to cite: *Angew. Chem. Int. Ed.* **2015**, *54*, 13245–13248
Angew. Chem. **2015**, *127*, 13443–13446

[1] a) R. G. Vogt in *Comprehensive Insect Science*, *Vol. 8* (Eds.: L. Gilbert, K. Iatrou, S. Gill), Elsevier, London, **2005**, p. 753; b) R. G. Vogt, L. M. Riddiford, *Nature* **1981**, *293*, 161; c) W. S. Leal, *Annu. Rev. Entomol.* **2013**, *58*, 373; d) P. Pelosi, J. J. Zhou, L. P. Ban, M. Calvello, *Cell. Mol. Life Sci.* **2006**, *63*, 1658; e) J. Fan, F. Francis, Y. Liu, J. L. Chen, D. F. Cheng, *GMR Genet. Mol. Res.* **2011**, *10*, 3056.

[2] a) P. Xu, R. Atkinson, D. N. Jones, D. P. Smith, *Neuron* **2005**, *45*, 193; b) T. Matsuo, S. Sugaya, J. Yasukawa, T. Aigaki, Y. Fuyama, *PLoS Biol.* **2007**, *5*, e118; c) S. Swarup, T. I. Williams, R. R. Anholt, *Genes Brain Behav.* **2011**, *10*, 648; d) Y. F. Sun, F. De Biasio, H. L. Qiao, I. Iovinella, S. X. Yang, Y. Ling, L. Riviello, D. Battaglia, P. Falabella, X. L. Yang, P. Pelosi, *PLOS ONE* **2012**, *7*, e32759.

[3] V. Campanacci, J. Krieger, S. Bette, J. N. Sturgis, A. Lartigue, C. Cambillau, H. Breer, M. Tegoni, *J. Biol. Chem.* **2001**, *276*, 20078.

[4] a) A. Schwaighofer, C. Kotlowski, C. Araman, N. Chu, R. Mastrogiacomo, C. Becker, P. Pelosi, W. Knoll, M. Larisika, C. Nowak, *Eur. Biophys. J.* **2014**, *43(2–3)*, 105–112; b) S. Paolini, F. Tanfani, C. Fini, E. Bertoli, P. Pelosi, *Biochim. Biophys. Acta Protein Struct. Mol. Enzymol.* **1999**, *1431*, 179–188; c) K. Matsumura, M. Opiekun, H. Oka, A. Vachani, S. M. Albelda, K. Yamazaki, G. K. Beauchamp, *PLOS ONE* **2010**, *5(1)*, e8819; d) M. Ghasemi-Varnamkhasti, S. S. Mohtasebi, M. Siadat, *J. Food Eng.* **2010**, *100*, 377–287; e) S. Schütz, B. Weißbecker, U. T. Koch, H. E. Hummel, *Biosens. Bioelectron.* **1999**, *14*, 221–228; f) W. Bourgeois, A.-C. Romain, J. Nicolas, R. M. Stuetz, *J. Environ. Monit.* **2003**, *5*, 852–860.

[5] a) S. J. Park, O. S. Kwon, S. H. Lee, H. S. Song, T. H. Park, J. Jang, *Nano Lett.* **2012**, *12*, 5082; b) H. J. Jin, S. H. Lee, T. H. Kim, J. Park, H. S. Song, T. Park, S. Hong, *Biosens. Bioelectron.* **2012**, *35*, 335; c) T. H. Kim, S. H. Lee, J. Lee, H. S. Song, E. H. Oh, T. H. Park, S. Hong, *Adv. Mater.* **2009**, *21*, 91; d) H. Yoon, S. H. Lee, O. S. Kwon, H. S. Song, E. H. Oh, T. H. Park, J. Jang, *Angew. Chem. Int. Ed.* **2009**, *48*, 2755; *Angew. Chem.* **2009**, *121*, 2793; e) F. Di Pietrantonio, D. Cannatà, M. Benetti, E. Verona, A. Varriale, M. Staiano, S. D'Auria, *Biosens. Bioelectron.* **2013**, *41*, 328; f) S. Sankaran, S. Panigrahi, S. Mallik, *Biosens. Bioelectron.* **2011**, *26*, 3103; g) S. D'Auria, V. Scognamiglio, M. Rossi, M. Staiano, S. Campopiano, N. Cennamo, L. Zeni in *Conference on Biomedical Vibrational Spectroscopy and Biohazard Detection Technologies*, *Vol. 5321*, SPIE—The International Society for Optical Engineering, San Jose California (USA), **2004**, p. 258.

[6] a) J. F. Huang, M. Larisika, W. H. D. Fam, Q. Y. He, M. A. Nimmo, C. Nowak, I. Y. A. Tok, *Nanoscale* **2013**, *5*, 2945; b) C. Y. Su, Y. Xu, W. Zhang, J. Zhao, X. Tang, C. H. Tsai, L. J. Li, *Chem. Mater.* **2009**, *21*, 5674–5680.

[7] V. K. Kodali, J. Scrimgeour, S. Kim, J. H. Hankinson, K. M. Carroll, W. A. de Heer, C. Berger, J. E. Curtis, *Langmuir* **2011**, *27*, 863–865.

[8] I. Iovinella, F. R. Dani, A. Niccolini, S. Sagona, E. Michelucci, A. Gazzano, S. Turillazzi, A. Felicioli, P. Pelosi, *J. Proteome Res.* **2011**, *10*, 3439.

[9] a) J. Golebiowski, J. Topin, L. Charlier, L. Briand, *Flavour Fragrance J.* **2012**, *27*, 445; b) L. Briand, C. Eloit, C. Nespoulous, V. Bézirard, J.-C. Huet, C. Henry, F. Blon, D. Trotier, J.-C. Pernollet, *Biochemistry* **2002**, *41*, 7241; c) L. Briand, C. Nespoulous, V. Perez, J.-J. Rémy, J.-C. Huet, J.-C. Pernollet, *Eur. J. Biochem.* **2000**, *267*, 3079.

[10] S. Spinelli, A. Lagarde, I. Iovinella, P. Legrand, M. Tegoni, P. Pelosi, C. Cambillau, *Insect Biochem. Mol. Biol.* **2012**, *42*, 41.

Received: June 21, 2015
Published online: September 14, 2015

